J Biol Inorg Chem (2013) 18:401–410
DOI 10.1007/s00775-013-0984-6

ORIGINAL PAPER

Functional models of α-keto acid dependent nonheme iron oxygenases: synthesis and reactivity of biomimetic iron(II) benzoylformate complexes supported by a 2,9-dimethyl-1,10-phenanthroline ligand

Oindrila Das · Sayanti Chatterjee · Tapan Kanti Paine

Received: 15 October 2012 / Accepted: 31 January 2013 / Published online: 16 February 2013

Abstract Two biomimetic iron(II) benzoylformate complexes, [$LFe^{II}(BF)_2$] (**2**) and [$LFe^{II}(NO_3)(BF)$] (**3**) (L is 2,9-dimethyl-1,10-phenanthroline and BF is monoanionic benzoylformate), have been synthesized from an iron(II)–dichloro complex [$LFe^{II}Cl_2$] (**1**). All the iron(II) complexes have been structurally and spectroscopically characterized. The iron(II) center in **2** is coordinated by a bidentate NN ligand (2,9-dimethyl-1,10-phenanthroline) and two monoanionic benzoylformates to form a distorted octahedral coordination geometry. One of the benzoylformates binds to the iron in **2** via both carboxylate oxygens but the other one binds in a chelating bidentate fashion via one carboxylate oxygen and the keto oxygen. On the other hand, the iron(II) center in **3** is ligated by one NN ligand, one bidentate nitrate, and one monoanionic chelating benzoylformate. Both iron(II) benzoylformate complexes exhibit the facial NNO donor environment in their solid-state structures. Complexes **2** and **3** are stable in noncoordinating solvents under an inert atmosphere, but react with dioxygen under ambient conditions to undergo oxidative decarboxylation of benzoylformate to benzoate in high yields. Evidence for the formation of an iron(IV)–oxo intermediate upon oxidative decarboxylation of benzoylformate was obtained by interception and labeling experiments. The iron(II) benzoylformate complexes represent the functional models of α-keto acid dependent oxygenases.

Keywords Iron · Benzoylformate · O–O activation · Decarboxylation · Functional models

Introduction

α-Ketoglutarate (α-KG)-dependent oxygenases are an important class of dioxygen-activating nonheme iron enzymes that exhibit a diverse range of biological activities [1–3]. The members of this superfamily of enzymes, in spite of their diverse reactivity, contain a common "2-His-1-carboxylate" facial triad in their active site and require an α-keto acid, iron(II), and O_2 [4–8]. X-ray crystallographic studies have provided useful information about the structures of this superfamily of enzymes. The α-keto acid dependent enzyme taurine dioxygenase (TauD), which catalyzes the hydroxylation of taurine, has been crystallographically characterized in three different forms [9]. The structure of the as-isolated form reveals the iron center with the "2-His-1-carboxylate" facial triad and three water molecules. The TauD–αKG form shows a bidentate binding of α-KG by replacement of two water molecules. The structure of the enzyme–α-KG–taurine complex reveals the binding of taurine to form a five-coordinate iron(II) center. The enzyme–α-KG–substrate complex allows the binding of dioxygen at the sixth coordination site to initiate the reaction. In a common mechanism for this class of nonheme enzymes, an iron(III)–superoxo intermediate has been proposed to form via activation of O_2 at the iron(II) α-keto acid center [1]. Subsequent O–O bond cleavage and decarboxylation of the iron–oxygen intermediate result in

Electronic supplementary material The online version of this article (doi:10.1007/s00775-013-0984-6) contains supplementary material, which is available to authorized users.

O. Das · S. Chatterjee · T. K. Paine (✉)
Department of Inorganic Chemistry,
Indian Association for the Cultivation of Science,
2A & 2B Raja S. C. Mullick Road,
Jadavpur 700032, Kolkata, India
e-mail: ictkp@iacs.res.in

formation of an iron(IV)–oxo intermediate, which has been shown experimentally to be the active oxidant in many oxygen-dependent transformation reactions [10–21]. The activation of dioxygen and the involvement of iron(IV)–oxo oxidant in the catalytic pathway of α-KG-dependent enzymes have been studied by theoretical calculations [16, 22–24].

Model complexes play an important role in understanding the nature of the intermediate species involved in the catalytic reaction pathway. Synthetic mononuclear Fe(IV)=O complexes supported by nonheme ligands have been isolated and characterized [25–30]. These Fe(IV)=O complexes exhibit versatile reactivity such as hydrogen-atom abstraction, hydroxylation, and oxo-atom transfer reactions [29, 31, 32]. A number of biomimetic iron α-keto acid complexes have been reported as models of α-keto acid dependent oxygenases in the literature. Most of the biomimetic complexes employed NNNN, NNNO, or NNN chelating ligands and different α-keto acids as model substrates [33–42]. Several nonheme iron complexes with NNO donor ligands have also been reported [43–50]. Additionally, the use of NN donors in combination with bulky carboxylates as "2-His-1-carboxylate" mimics has been documented in the literature [51]. However, examples of biomimetic complexes with the NNO facial triad as models for α-keto acid dependent oxygenases are rare [52].

We have initiated a project on the development of biomimetic iron complexes using substituted 1,10-phenanthrolines. 1,10-Phenanthrolines are oxidatively robust and find applications in bioinspired catalysis. The oxo-bridged diiron(III) complexes of 1,10-phenanthroline have been used as catalysts for alkene epoxidation, sulfide oxidation, and alkane hydroxylation using peroxides as oxidants [53–56]. However, there is no report of an iron(II) phenanthroline complex acting as a functional model of oxygen-activating nonheme iron enzymes. As an outcome of our work in this direction, we report herein the synthesis and structural characterization of two mononuclear iron(II) benzoylformate complexes, [$LFe^{II}(BF)_2$] (**2**) and [$LFe^{II}(NO_3)(BF)$] (**3**), where L is 2,9-dimethyl-1,10-phenanthroline and BF is monoanionic benzoylformate. Both model iron(II) benzoylformate complexes exhibit the facial NNO donor environment as observed from their X-ray single-crystal structures. The dioxygen activation by the iron(II) benzoylformate complexes and the mechanistic studies of oxidative decarboxylation of benzoylformate are reported.

Materials and methods

All chemicals were purchased from commercial sources. Solvents were distilled and dried before use. The synthesis and manipulation of air-sensitive complexes were done under a nitrogen environment in an inert atmosphere glove box. Fourier transform infrared (FT-IR) spectra were recorded using a Shimadzu FT-IR 8400S instrument. Elemental analyses were performed with a PerkinElmer 2400 series II CHN analyzer. Solution electronic spectra were measured at room temperature with an Agilent 8453 diode-array spectrophotometer. Electrospray ionization mass spectra were recorded with a Waters QTOF Micro YA263 system. ^{1}H NMR spectra were measured using a Bruker Avance III 500-MHz spectrometer. Room temperature magnetic data were collected with a Gouy balance (Sherwood Scientific, Cambridge, UK). Diamagnetic contributions were estimated for each compound by using Pascal's constants. Gas chromatography (GC)–mass spectrometry (MS) measurements were conducted with a PerkinElmer Clarus 680 GC and SQ8T MS system, using an Elite 5 MS column (30 m × 0.25 mm × 0.25 μm) with 300 °C maximum temperature. Labeling experiments were conducted with $^{18}O_2$ gas (99 atom %) or $H_2{}^{18}O$ (98 atom %) from Icon Services (USA).

For synthesis of [$LFe^{II}Cl_2$] (**1**), 2,9-dimethyl-1,10-phenanthroline (0.104 g, 0.5 mmol) was reacted with $FeCl_2$ (0.0633 g, 0.5 mmol) in dry dichloromethane (10 mL) at room temperature. The resulting solution was stirred for 30 min to precipitate a yellow solid. The solid was isolated by filtration. X-ray-quality single crystals of the complex were isolated from a solvent mixture of dichloromethane and diethyl ether. Yield: 0.15 g (90 %). Anal Calcd for $C_{14}H_{12}Cl_2FeN_2$ (335.01 g mol^{-1}): C, 50.19; H, 3.61; N, 8.36 %. Found: C, 50.16; H, 3.55; N, 8.38 %. FT-IR (KBr) (cm^{-1}): 3,422 (br), 3,067 (w), 2,924 (w), 2,855 (vw), 1,622 (m), 1,591 (s), 1,566 (m), 1,504 (vs), 1,425 (m), 1,379 (w), 1,296 (w), 1,222 (m), 1,153 (m), 1,036 (s), 864 (vs), 781 (s), 729 (s). UV–vis (dichloromethane) [λ_{max}, nm (ε, M^{-1} cm^{-1})]: 335 (sh). μ_{eff} (20 °C): 5.09 μ_B.

For synthesis of [$LFe^{II}(BF)_2$] (**2**), a dichloromethane solution (15 mL) of **1** (0.1675 g, 0.5 mmol) was treated with sodium benzoylformate (0.172 g, 1 mmol). The solution was stirred at room temperature for 12 h, during which time the solution turned violet. The solution was then filtered and the filtrate was kept for layer diffusion with diethyl ether to isolate X-ray-quality single crystals of **2**. Yield: 0.16 g (60 %). Anal Calcd for $C_{30}H_{22}FeN_2O_6$ (562.35 g mol^{-1}): C, 64.06; H, 3.94; N, 4.98. Found: C, 64.18; H, 3.86; N, 5.03 %. FT-IR (KBr) (cm^{-1}): 3,450 (br), 3,070 (w), 2,924 (w), 1,672 (vs), 1,627 (vs), 1,593 (vs), 1,504 (m), 1,444 (m), 1,431 (m), 1,385 (w), 1,234 (vs), 1,176 (m), 1,153 (w), 1,001 (m), 860 (m), 815 (m), 715 (m), 681 (s). UV–vis (dichloromethane) [λ_{max}, nm (ε, M^{-1} cm^{-1})]: 580 (550), 528 (620), 480 (sh). μ_{eff} (20 °C): 4.76 μ_B.

For synthesis of [$LFe^{II}(NO_3)(BF)$] (**3**), a dichloromethane solution (15 mL) of **1** (0.1675 g, 0.5 mmol) was

treated with a mixture of sodium benzoylformate (0.086 g, 0.5 mmol) and $AgNO_3$ (0.127 g, 0.75 mmol). The solution was stirred for 12 h, during which time the solution turned violet. The violet solution was then filtered and the filtrate was kept for layer diffusion with hexane to isolate a purple crystalline solid. Yield: 0.099 g (42 %). Anal Calcd for $C_{22}H_{17}FeN_3O_6$ (475.23 g mol^{-1}): C, 55.60; H, 3.61; N, 8.84. Found: C, 55.53; H, 3.47; N, 9.01 %. FT-IR (KBr) (cm^{-1}): 3,435 (br), 3,065 (w), 1,684 (vs), 1,630 (vs), 1,591 (vs), 1,506–1,477 (s), 1,383 (vs), 1,288 (s), 1,230 (vs), 1,175 (m), 1,155 (m), 1,026 (m), 1,001 (m), 987 (m), 862 (s), 818 (m), 775 (w), 752 (m), 729 (m), 685 (s). UV–vis (dichloromethane) [λ_{max}, nm (ε, M^{-1} cm^{-1})]: 580 (335), 525 (400), 490 (435). μ_{eff} (20 °C): 4.83 μ_B.

Reactivity with dioxygen

The iron(II) benzoylformate complex (0.02 mmol) was dissolved in 10 mL dry solvent (dichloromethane or acetonitrile). Pure oxygen gas was bubbled through the solution for 3 min, and the solution was then stirred at room temperature under an oxygen atmosphere. The light-orange solution thus formed was dried by use of a rotary evaporator to remove the solvent, and the residue was treated with 3.0 M HCl solution (10 mL). The organic products were then extracted with diethyl ether (3 × 15 mL), dried over anhydrous Na_2SO_4, and analyzed by ^{1}H NMR spectroscopy in $CDCl_3$. A control experiment was performed in the absence of the iron complex by analyzing a solution of sodium benzoylformate under oxygen with stirring for 20 h. No appreciable decomposition of benzoylformate was observed in the control experiment.

Interception studies with phenols

The iron(II) benzoylformate complex (0.02 mmol) was dissolved in 10 mL dry acetonitrile. To the solution was added 10 equiv of phenols (0.2 mmol). Pure oxygen gas was bubbled through the solution for 3 min, and the solution was then stirred at room temperature under an oxygen atmosphere for 20 h. The reaction solution was then dried by use of a rotary evaporator, and the residue was treated with 3.0 M HCl solution (10 mL). The organic products were extracted with diethyl ether (3 × 15 mL) and dried over Na_2SO_4. The ether solution was then filtered through a silica gel column and washed several times with diethyl ether. The solvent was removed from the filtrate, dried under a vacuum, and the organic products were characterized by ^{1}H NMR spectroscopy.

Organic product derived from 2,4-di-*tert*-butylphenol

^{1}H NMR data of 4,4′,6,6′-tetra-*tert*-butyl-2,2′-biphenol (500 MHz, $CDCl_3$; δ, ppm): 1.32 (s, 18H), 1.45 (s, 18H), 5.28 (s, 2H), 7.11 (d, $J = 2.5$ Hz, 2H), 7.40 (d, $J = 2.5$ Hz, 2H). The yield of biphenol was calculated on the basis of starting Fe(II) complexes: 60 and 45 % with **2** and **3**, respectively. Control experiments were also performed in the absence of iron complexes. No biphenol was formed in the control experiments.

Organic product derived from 2,4,6-tri-*tert*-butylphenol

^{1}H NMR data of 2,6-di-*tert*-butyl-1,4-benzoquinone (500 MHz, $CDCl_3$; δ, ppm): 1.27–1.28 (br, 18H), 6.51 (s, 2H). Yield: 90 % for **2** and 75 % for **3**.

Interception studies with dimethyl sulfide/dimethyl sulfoxide

The iron(II) benzoylformate complex (0.02 mmol) was dissolved in dry acetonitrile (10 mL). To the solution was added 10 equiv of external substrates (0.2 mmol). Pure oxygen gas was bubbled through the solution for 3 min, and the solution was stirred at room temperature under an oxygen atmosphere for 20 h. The solvent was then removed from the reaction mixture and distilled benzene was added. A slight excess of sodium dithionite (0.04 mmol) was then added to the benzene solution, followed by addition of D_2O, and the resulting solution was stirred for 30 min. To the solution was added 1,10-phenanthroline monohydrate (0.06 mmol), and the solution was then stirred for an additional 15 min. The D_2O layer was then collected and analyzed by ^{1}H NMR spectroscopy. ^{1}H NMR data of dimethyl sulfoxide derived from dimethyl sulfide (500 MHz, D_2O; δ, ppm) 2.74 (s, 6H). Yield: 33 % for **2** and 23 % for **3**. ^{1}H NMR data of dimethyl sulfone from dimethyl sufoxide (500 MHz, D_2O; δ, ppm) 3.17 (s, 6H). Yield: 18 % for **2**. Control experiments were also performed in the absence of iron complexes. No oxidation of external substrates occurred in the control experiments.

X-ray crystallographic data collection and refinement of the structures

Diffraction data for **1**, **2**, and **3** were collected at 20 °C with Mo Kα radiation ($\lambda = 0.71073$ Å). Each crystal was fixed on the tip of a glass capillary and mounted on a on a Bruker Smart APEX II CCD diffractometer. Crystallographic data for the complexes are summarized in Table 1. Cell refinement, indexing, and scaling of the data sets were done using APEX2, version 2.1-0 [57]. The structures were solved by the Patterson method and subsequent Fourier

Table 1 Crystallographic data of $[LFe^{II}Cl_2]$ (**1**), $[LFe^{II}(BF)_2]$ (**2**), and $[LFe^{II}(NO_3)(BF)]$ (**3**), where L is 2,9-dimethyl-1,10-phenanthroline and BF is monoanionic benzoylformate

Crystal parameters	**1**	**2**	**3**
Empirical formula	$C_{14}H_{12}Cl_2FeN_2$	$C_{30}H_{22}FeN_2O_6$	$C_{22}H_{17}FeN_3O_6$
Formula weight	335.01	562.35	475.24
Crystal system	Orthorhombic	Triclinic	Monoclinic
Space group	*Pnma*	*P*-1	$P2_1/c$
a (Å)	11.2381 (7)	8.494 (2)	15.581 (14)
b (Å)	7.5280 (5)	10.793 (2)	7.163 (6)
c (Å)	17.8070 (11)	15.107 (4)	17.791 (15)
α (°)	90	93.887 (10)	90
β (°)	90	104.292 (8)	94.432 (12)
γ (°)	90	109.261 (6)	90
Volume (Å^3)	1,506.48 (17)	1,250.1 (5)	1,980 (3)
Z	4	2	4
D_{calc} (g cm^{-3})	1.477	1.494	1.594
F(000)	680	580.0	976.0
μ Mo Kα (mm^{-1})	1.342	0.653	0.810
Temperature (K)	293 (2)	293 (2)	293 (2)
R_{int}	0.0363	0.0359	0.0781
θ range data collection (°)	2.14–27.74	1.41–25.00	1.31–19.65
Reflections collected	15,315	14,219	6,929
Unique reflections	1,893	4,394	1,691
Observed reflections [$I > 2\sigma(I)$]	1,434	3,641	1,066
Parameters	114	354	286
Goodness of fit on F^2	0.862	1.098	1.059
Final *R* indices [$I > 2\sigma(I)$]	$R_1 = 0.0335$ $wR_2 = 0.1101$	$R_1 = 0.0355$ $wR_2 = 0.0952$	$R_1 = 0.0552$ $wR_2 = 0.1401$
R indices (all data)	$R_1 = 0.0491$ $wR_2 = 0.1243$	$R_1 = 0.0459$ $wR_2 = 0.1019$	$R_1 = 0.0946$ $wR_2 = 0.1676$

analyses and refined by the full-matrix least-squares method based on F^2 with all observed reflections. All non-hydrogen atoms were refined anisotropically and hydrogen atoms were placed in ideal positions. All the calculations were performed using the WinGX system, version 1.80.05 [58]. Complex **3** diffracts at low angle with poor resolution of the data set as a distinctive feature of the crystals. The final full-matrix least-squares refinement on F^2 converged to $R_1 = 0.0335$ and $wR_2 = 0.1243$ for **1**, $R_1 = 0.0355$ and $wR_2 = 0.1019$ for **2**, and $R_1 = 0.0552$ and $wR_2 = 0.1676$ for **3**. The N3 nitrogen atom of nitrate ion in **3** exhibits non-positive-definite displacement in an anisotropic refinement and was refined isotropically.

Results and discussion

Synthesis and characterization

The iron(II) benzoylformate complexes were synthesized from a precursor iron(II)–chloro complex. The precursor complex **1** was prepared by mixing $FeCl_2$ with 2,9-dimethyl-1,10-phenanthroline in dichloromethane [59, 60]. The ^{1}H NMR spectrum (Fig. S1) of **1** in $CDCl_3$ displays paramagnetically shifted proton resonances typical of high-spin iron(II) complexes as observed in the analogous complex $[(dmby)FeCl_2]$ (dmby is 6,6′-dimethyl-2,2′-bipyridine) [61]. The room temperature effective magnetic moment of 5.09 μ_B for **1** is in good agreement with the spin-only value calculated for high-spin iron(II) complexes [62].

The complex was further characterized by single-crystal X-ray diffraction studies. X-ray-quality single crystals of **1** were grown from a solvent mixture of dichloromethane and diethyl ether. The single-crystal structure of the neutral complex confirmed an iron(II) center coordinated by a bidentate NN donor ligand (2,9-dimethyl-1,10-phenanthroline) and two chlorides, resulting in a tetrahedral coordination geometry (Fig. 1). The iron–nitrogen and iron–chloro distances (Table 2) are typical of high-spin iron(II) complexes and are in the range of those reported for $[(dmby)FeCl_2]$ [61].

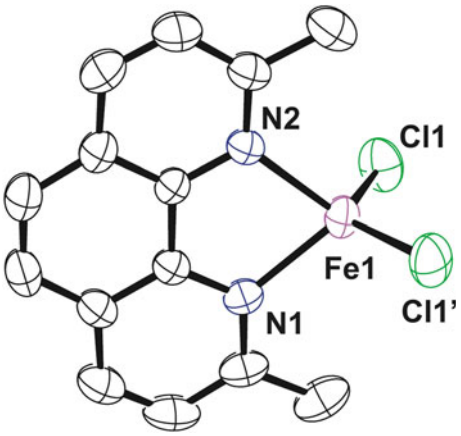

Fig. 1 ORTEP plot (40 % probability of thermal ellipsoids) of $[LFe^{II}Cl_2]$ (**1**), where L is 2,9-dimethyl-1,10-phenanthroline. All hydrogen atoms have been omitted for clarity

Table 2 Selected bond distances (Å) and angles (°) for **1**

Fe1–N1	2.111 (3)	Fe1–N2	2.120 (2)
Fe1–Cl1	2.2209 (6)		
N1–Fe1–N2	79.06 (9)	N1–Fe1–Cl1	112.22 (3)
N2–Fe1– Cl1	111.07 (3)	Cl1–Fe1–Cl1	122.83 (4)

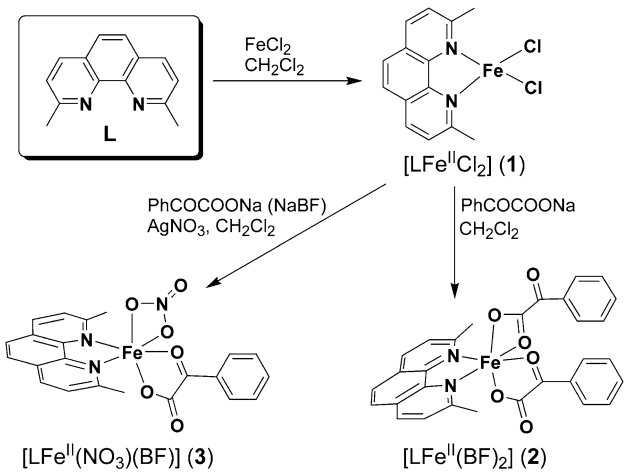

Scheme 1 Syntheses of iron(II) benzoylformate complexes

Complex **2** was isolated from the reaction of **1** with 2 equiv of sodium benzoylformate. When 1 equiv of sodium benzoylformate was used in the reaction, the yield of **2** was found to be low as a result of the isolation of unreacted **1** from the reaction solution. Complex **3** was prepared from **1** using equimolar amounts of reagents in the presence of 1.5 equiv of $AgNO_3$ (Scheme 1).

The complexes were characterized by different spectroscopic and analytical techniques. Both iron(II) benzoylformate complexes show strong infrared peaks in the 1,680–1,590-cm^{-1} region, indicating the binding of α-keto acid anion. The bidentate binding of benzoylformate was supported by the characteristic purple-to-violet color of the complexes in dichloromethane with λ_{max} values falling in the region of 500–600 nm (Fig. 2) [33, 38, 63]. These features in the optical spectra, by analogy to reported data, are assigned to the iron(II) to α-keto acid charge transfer transition. In α-KG-dependent TauD, the charge transfer transition has been observed at 530 nm in the presence of iron(II) and α-KG under anaerobic conditions [1]. Room temperature magnetic moments of 4.76 and 4.83 μ_B for **2** and **3**, respectively, suggest the high-spin nature of the iron(II) complexes. The mononuclear iron(II) benzoylformate complexes are stable under a nitrogen atmosphere.

To determine the binding affinity of benzoylformate for LFe(II) in solution, optical spectral titrations were performed by gradual addition of sodium benzoylformate to a dichloromethane solution of **1** under an inert atmosphere. The intensity of the characteristic metal to α-keto acid charge transfer transitions at 580 and 528 nm increases linearly with the concentration of sodium benzoylformate. The intensity of the metal-to ligand charge transfer (MLCT) band attains a maximum value after addition of 1.4 equiv of sodium benzoylformate and remains unaltered upon further addition of the α-keto acid (Fig. 3). The loss of MLCT intensity in acetonitrile is due to the coordination

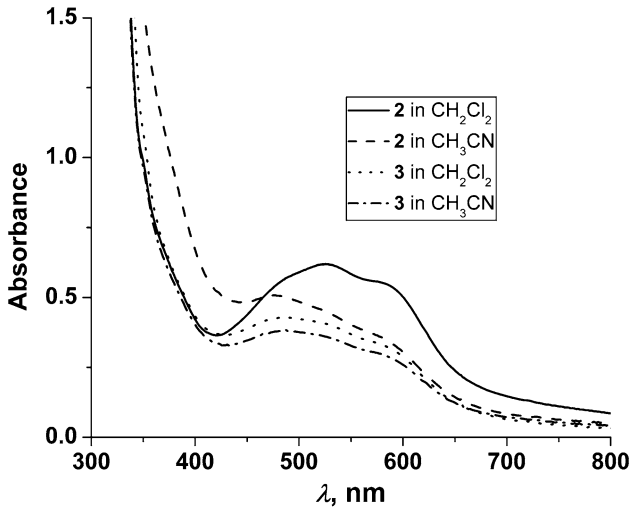

Fig. 2 Optical spectra at 23 °C of 1 mM [$LFe^{II}(BF)_2$] (**2**) and 1 mM [$LFe^{II}(NO_3)(BF)$] (**3**), where L is 2,9-dimethyl-1,10-phenanthroline and BF is monoanionic benzoylformate

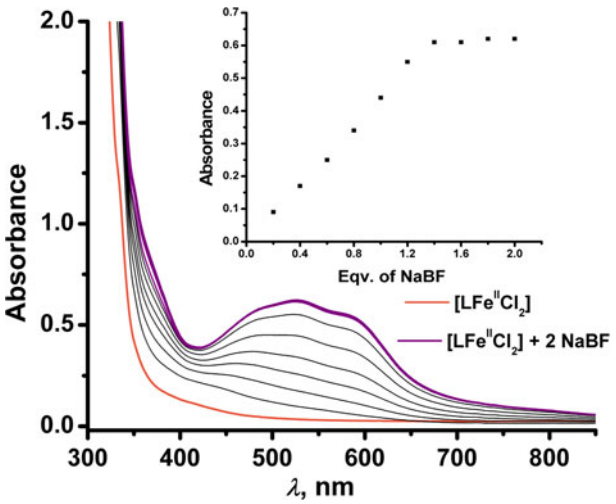

Fig. 3 Changes in optical spectra on addition of sodium benzoylformate (*NaBF*) in methanol to a dichloromethane solution of **1** (1 mM) at 23 °C. *Inset*: Absorbance at 528 nm versus number of equivalents of sodium benzoylformate added

of solvent, which possibly causes a change of the κ^2-benzoylformate coordination to a κ^1-benzoylformate coordination (Fig. 2) [33]. The resonances for benzoylformate protons appear between 20.00 and 7.50 ppm in the ^1H NMR spectra of the iron(II) benzoylformate complexes. The peak positions of benzoylformate protons in CD_3CN and $CDCl_3$ support a change in coordination mode of benzoylformate in acetonitrile (Figs. S2–S5).

To obtain a structural understanding of the complexes, single crystals were grown from a solvent mixture of dichloromethane and diethyl ether (for **2**) or dichloromethane and hexane (for **3**). The X-ray single crystal structure of the neutral complex **2** reveals a six-coordinate

mononuclear iron complex representing the crystallographic asymmetric unit (Fig. 4). The iron center is coordinated by a bidentate ligand and two monoanionic benzoylformates. One of the benzoylformates binds to the metal center via both the carboxylate oxygens, whereas the other benzoylformate coordinates in a chelating bidentate fashion through one carboxylate oxygen and the carbonyl oxygen. The two nitrogen donors (N1 and N2) of the bidentate ligand and the oxygen donor (O5) of the carboxylate group of one of the coordinated benzoylformates constitute the facial triad as described in the "2-His-1-carboxylate" structural motif in the active site of α-KG-dependent metalloenzymes. The other face of the coordination sphere is occupied by the carboxylate oxygen (O4), the keto oxygen (O3), and carboxylate oxygen (O2) of the chelating benzoylformate. The pyridine nitrogen (N1) and the keto oxygen (O3) of benzoylformate occupy the axial positions, with an N1–Fe1–O3 angle of 161.37 (6)° (Table 3). The other pyridine nitrogen (N2), carboxylate oxygen (O2) of benzoylformate, and two carboxylate oxygens (O4 and O5) of the other benzoylformate occupy equatorial sites, with N2–Fe1–O4 and O2–Fe1–O5 angles of 147.58 (7)° and 155.93 (7)°, respectively. The Fe–N bond distances [2.188 (2) and 2.154 (2) Å] are typical of a high-spin iron (II) complex [52]. The five-membered chelate ring at the iron(II) center formed by the chelating benzoylformate contains two different Fe–O bonds, i.e., Fe–O(keto) of 2.2630 (16) Å and Fe–O(carboxylate) of 1.9986 (17) Å, similar to those observed in other iron(II) benzoylformate complexes [33, 35, 38]. A four-membered chelate ring is formed by the asymmetrically coordinated carboxylate group of a benzoylformate with Fe1–O4 and Fe1–O5 distances of 2.335 (2) and 2.1350 (17) Å, respectively. The benzoylformate chelate is almost coplanar with the phenyl ring, exhibiting a dihedral angle of 16.48°. In contrast, both benzoylformates bind in a bidentate chelating fashion in a related complex, [(dmby)Fe$(BF)_2$], where the chelate rings at the metal center deviate from planarity as a result of the intramolecular face-to-face "$\pi\cdots\pi$" interaction between the phenyl rings of the two benzoylformates [52].

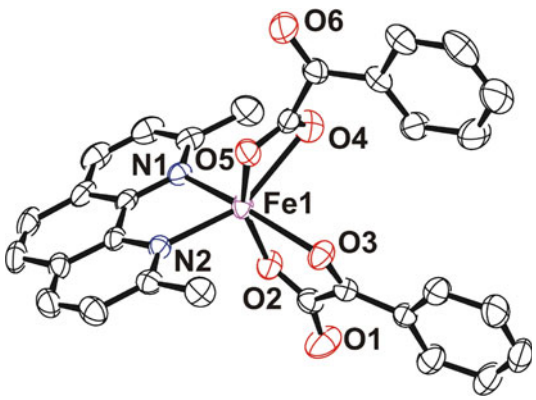

Fig. 4 ORTEP diagram of **2** with thermal ellipsoids drawn at the 40 % probability level. All hydrogen atoms have been omitted for clarity

Table 3 Selected bond distances (Å) and angles (°) for **2**

Fe(1)–N(1)	2.1875 (17)	Fe(1)–O(3)	2.2630 (16)
Fe(1)–N(2)	2.1537 (18)	Fe(1)–O(4)	2.335 (2)
Fe(1)–O(2)	1.9986 (17)	Fe(1)–O(5)	2.1350 (17)
N(1)–Fe(1)–N(2)	77.66 (7)	O(2)–Fe(1)–O(3)	73.48 (6)
O(5)–Fe(1)–O(4)	57.91 (7)	N(1)–Fe(1)–O(3)	161.37 (6)
N(2)–Fe(1)–O(4)	147.58 (7)	O(2)–Fe(1)–O(5)	155.93 (7)
O(2)–Fe(1)–N(2)	100.43 (7)	O(5)–Fe(1)–N(2)	92.27 (7)
O(2)–Fe(1)–N(1)	88.53 (7)	O(5)–Fe(1)–N(1)	114.30 (7)
O(5)–Fe(1)–O(3)	83.03 (6)	N(2)–Fe(1)–O(3)	109.77 (7)
O(2)–Fe(1)–O(4)	111.99 (7)	N(1)–Fe(1)–O(4)	101.83 (7)
O(3)–Fe(1)–O(4)	81.14 (7)		

Although the diffraction data for **3** were obtained at low θ angle with poor resolution of the data set, the structural determination allowed us to clarify some relevant geometrical features (Fig. S6). The iron center in **3** is coordinated by a bidentate ligand (2,9-dimethyl-1,10-phenanthroline), one monoanionic bidentate nitrate, and one monoanionic chelated benzoylformate. In this case, two nitrogen donors (N1 and N2) of 2,9-dimethyl-1,10-phenanthroline and an oxygen donor (O5) of the bidentate nitrate form the NNO facial triad. Pyridine nitrogen N1 and keto oxygen O3 occupy the axial positions of the distorted octahedral coordination geometry around the iron(II) center. The chelating benzoylformate shows a slightly stronger Fe–O(keto) bond, with a length of 2.210 (7) Å (Table S1), possibly due to better conjugation of the keto group with the phenyl ring. This is also reflected in a small dihedral angle value of 10.49° between the bidentate benzoylformate chelate and the phenyl ring.

Reactivity with dioxygen

Both iron(II) benzoylformate complexes (**2** and **3**) are reactive towards dioxygen. The reactivities of **2** and **3** were studied in acetonitrile and in dichloromethane. Complex **2** reacts slowly with dioxygen in acetonitrile over a period of 20 h. The reaction was monitored by analyzing the organic products with time (Fig. 5). The ^{1}H NMR and GC–MS spectra of the organic products from **2** after removal of the metal ion by acidic workup of the reaction solution show almost quantitative conversion of benzoylformic acid to benzoic acid after 20 h (Fig. 5, Fig. S7).

In dichloromethane, complex **2** reacts with dioxygen for 20 h, during which the characteristic purple color, originating from MLCT bands at 580 and 528 nm, slowly decays to light orange following pseudo-first-order kinetics

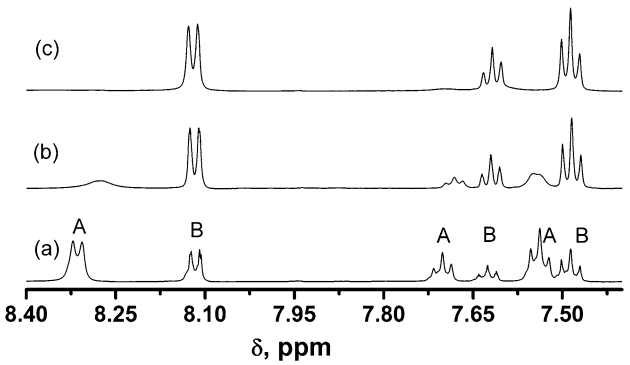

Fig. 5 ^{1}H HMR spectra of organic products after *a* 2 h, *b* 5 h, and *c* 20 h reaction of **2** with dioxygen in acetonitrile at 23 °C. Peaks marked as *A* are from benzoylformic acid and peaks marked as *B* are from benzoic acid

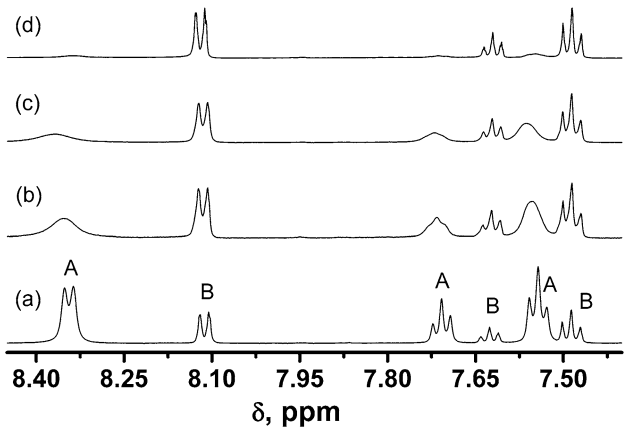

Fig. 6 ^{1}H NMR spectra of organic products after *a* 3 h, *b* 5 h, *c* 8 h, and *d* 16 h reaction of **3** with dioxygen in acetonitrile at 23 °C. Peaks marked as *A* are from benzoylformic acid and peaks marked as *B* are from benzoic acid

(Fig. S8). The ^{1}H NMR spectrum of the reaction solution reveals the oxidative decarboxylation of benzoylformic acid to benzoic acid in quantitative yield. Similarly, complex **3** reacts with dioxygen in acetonitrile to give almost quantitative yield of benzoic acid after 20 h (Fig. 6). During the reaction, the MLCT bands at 525 and 580 nm slowly decay following pseudo-first-order kinetics (Fig. S9). A dichloromethane solution of **3** slowly reacts with dioxygen under ambient conditions, during which the light-purple solution changes to a light-yellow solution. The ^{1}H NMR spectrum of the organic products after removal of the metal ion reveals almost complete conversion of benzoylformic acid to benzoic acid.

The reaction of **2** with $^{18}O_2$ was performed to understand the fate of oxygen atoms from molecular oxygen. The analysis of organic product by GC–MS clearly suggests the incorporation of one labeled oxygen atom from $^{18}O_2$ into benzoic acid during the decarboxylation of benzoylformate (Fig. S10). The iron(II) benzoylformate complexes are therefore functional mimics of α-keto acid dependent enzymes.

To understand the involvement of the iron–oxygen intermediate in the decarboxylation pathway of iron(II) benzoylformate complexes, the reaction of **2** (or **3**) with dioxygen was conducted at −40 °C in acetonitrile. No feature for any iron–oxygen intermediate species was observed spectrophotometrically under the experimental conditions; therefore the reactions were studied in the presence of external probes such as thioanisole, dimethyl sulfide, dimethyl sulfoxide, dihydroanthracene, 2,4-di-*tert*-butylphenol, and 2,4,6-tri-*tert*-butylphenol to intercept metal–oxygen species. Iron(III) superoxide and copper(II) superoxide intermediates are known to cleave the O–H bond of phenols homolytically [33, 40, 64, 65]. The ^{1}H NMR spectra of the organic products derived from 2,4-di-*tert*-butylphenol after the reaction suggest the formation of 3,3′,5,5′-tetra-*tert*-butyl-2,2′-biphenol in 60 and 45 % yield with **2** and **3**, respectively (Scheme 2). This result supports the formation of a phenoxyl radical by abstraction of a hydrogen atom of phenol by an iron–oxygen intermediate. Similarly, 2,4,6-tri-*tert*-butylphenol affords 2,6-di-*tert*-butylbenzoquinone (90 % and 75 % yield with **2** and **3**, respectively) as a result of the decomposition of 2,4,6-tri-*tert*-butylphenoxyl radical formed in situ on hydrogen-atom abstraction. The formation of 2,4,6-tri-*tert*-butylphenoxyl radical in the interception reaction was proved by X-band EPR spectroscopy. Of note, the presence of external substrates does not affect the decarboxylation of benzoylformate.

Although no interception is observed in the presence of thioanisole or dihydroanthracene, reaction of iron(II) benzoylformate complex **2** with dioxygen in the presence of dimethyl sulfide affords dimethyl sulfoxide in 33 % yield. When dimethyl sulfoxide is used as intercepting reagent, 18 % dimethyl sulfone is formed as the only product (Fig. S11). Additionally, decarboxylation of **2** with $^{18}O_2$ in the presence of dimethyl sulfoxide affords sulfone, where one labeled oxygen atom is incorporated into sulfone and the other one is incorporated into benzoic acid (Figs. S10, S12). Moreover, addition of $H_2{}^{18}O$ in the reaction of **2** with $^{16}O_2$ in the presence of sulfoxide results in about 10 % incorporation of ^{18}O into sulfone (Fig. S13). These results support the formation of an iron(IV)–oxo intermediate during the decarboxylation of benzoylformate. The iron(IV)–oxo, exchangeable with water, is involved in oxo-atom transfer to dimethyl sufide/sulfoxide, resulting in the formation of dimethyl sulfoxide/sulfone and O–H atom abstraction from phenols (Scheme 2).

Oxidative decarboxylation of the α-keto acid substrate has been observed upon oxygenation of several biomimetic iron(II) benzoylformate complexes with N_3 and N_4 donor ligands. An in situ generated complex—[(Tp^{Me2})Fe(BF)],

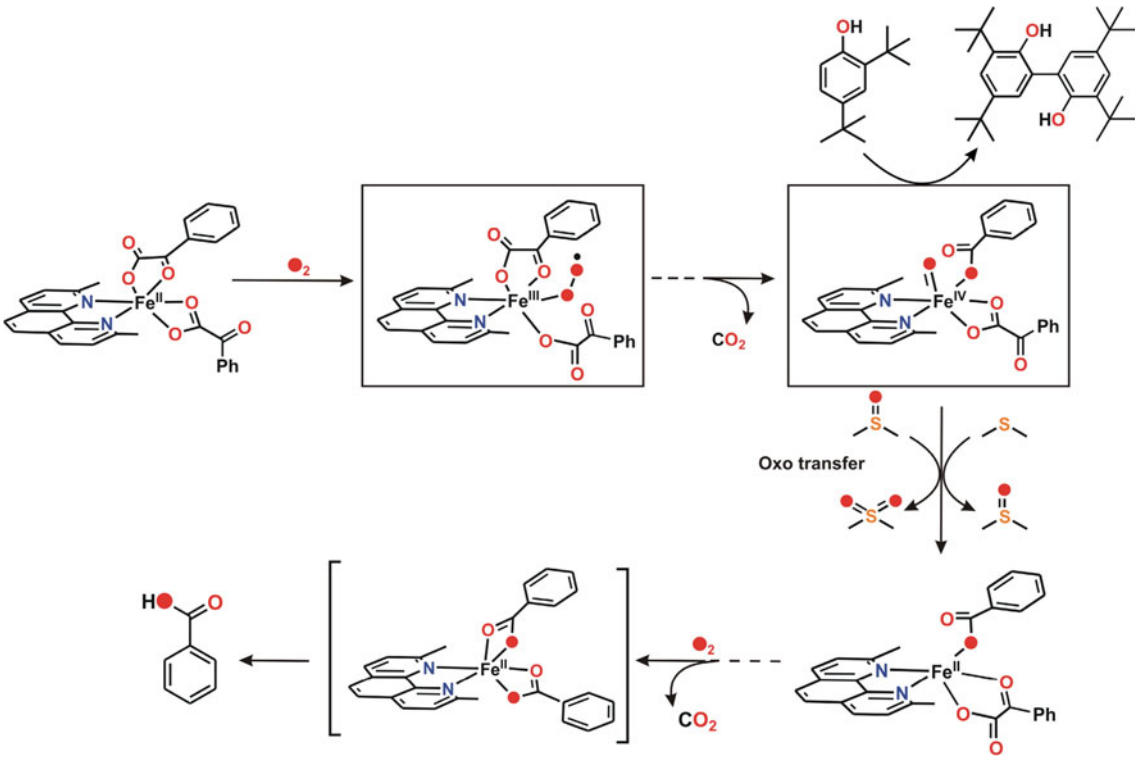

Scheme 2 Proposed pathway for oxidative decarboxylation of iron(II) benzoylformate complex **2**

where Tp^{Me2} is hydrotris(3,5-dimethylpyrazol-1-yl)borate—of a monoanionic facial N_3 donor ligand has been shown to carry out epoxidation of *cis*-stilbene in the presence of dioxygen [34]. Another iron(II) benzoylformate complex—[(Tp^{Ph2})Fe(BF)], where Tp^{Ph2} is hydrotris(3,5-diphenylpyrazol-1-yl)borate—reacts with dioxygen to undergo oxidative decarboxylation of benzoylformate with concomitant hydroxylation of one of the phenyl rings on the ligand backbone [38]. Model iron(II) benzoylformate complexes $[(6Me_3TPA)Fe(BF)]^+$ and $[(TPA)Fe(BF)(MeOH)]^+$ with tripodal N_4 donor ligands, where $6Me_3TPA$ is tris[(6-methyl-2-pyridyl)methyl]amine and TPA is tris(2-pyridylmethyl)amine, show quantitative decarboxylation of benzoylformate to benzoate upon exposure to dioxygen [33]. A model iron(II) benzoylformate complex, $[(dmby)Fe(BF)_2]$, with a facial NNO coordination environment has recently been shown to undergo oxidative decarboxylation of benzoylformate but with a low yield of benzoic acid [52]. In spite of the slow reaction, the high yield of benzoic acid with the present system is an improvement over the yield with the previously reported iron(II) benzoylformate complex with the facial NNO donor environment. Moreover, the biomimetic iron(II) complexes reported here differ from most common model complexes that rely on nitrogen-rich ligands.

The five-membered chelate ring formed upon bidentate binding of benzoylformate prefers to adopt a planar geometry. The second benzoylformate, if bound in a chelating mode, would face steric interactions with the two methyl groups of the planar ligand, 2,9-dimethyl-1,10-phenanthroline. To avoid the steric interaction, the second benzoylformate coordinates to the iron center through the carboxylate oxygens. The optical spectral data (Fig. 2) indicate the existence of a dynamic equilibrium in solution between the species containing benzoylformate ligated to the iron(II) center with different binding motifs. In solution, a five-coordinate iron(II) species (with a monodentate benzoylformate in **2** and a monodentate nitrate in **3**) is therefore proposed to activate dioxygen to form an iron(III) superoxide intermediate (Scheme 2). The chelated benzoylformate is expected to undergo oxidative decarboxylation; the yield of benzoic acid would be at maximum 50 % with respect to two benzoylformates. A quantitative yield of benzoic acid in acetonitrile suggests the participation of both benzoylformates in dioxygen activation. The iron(III) superoxide anion attacks the keto carbon to effect the decarboxylation of benzoylformate with concomitant formation of an iron(IV)–oxo species. The active oxidant then oxidizes external substrates such as substituted phenols, sulfides, and sulfoxides. The isolation of 2,9-dimethyl-1,10-phenanthroline quantitatively after the reaction indicates that the ligand remains unaffected during the oxidative transformation. The benzoate formed in the decarboxylation reaction may coordinate to the iron center

and the second benzoylformate may then realign itself to bind as a chelating ligand for further oxygen activation and decarboxylation. The resulting iron(II) benzoate complexes most likely are oxidized further to iron(III) compounds. Unfortunately, all attempts to isolate the final oxidized iron compounds failed in both cases.

Conclusion

We have isolated and structurally characterized two biomimetic iron(II) benzoylformate complexes supported by a 1,10-phenanthroline-based ligand. The facial NNO ligand environment, provided by a bidentate NN donor ligand and an O donor from either benzoylformate or nitrate, with a coordinated benzoylformate in ternary iron(II) complexes structurally mimics the "2-His-1-carboxylate" facial triad motif observed in the superfamily of nonheme iron enzymes. Both iron(II) benzoylformate complexes react with dioxygen to show oxidative decarboxylation of benzoylformic acid in high yield and functionally mimic the nonheme α-keto acid dependent enzymes. An iron(III) superoxide radical intermediate has been proposed to initiate the reaction leading to the formation of an Fe(IV)=O species. Indirect evidence for the formation of an Fe(IV)=O intermediate in the decarboxylation reaction was obtained by interception studies using different external reagents. The results demonstrate the role played by the phenanthroline-derived ligand in providing the necessary structural and electronic environment to carry out the oxidative decarboxylation reaction.

Acknowledgments We are grateful to the Department of Science and Technology (DST), Government of India, for financial support (project SR/SI/IC-51/2010). X-ray diffraction data were collected at the DST-funded National Single Crystal Diffractometer Facility at the Department of Inorganic Chemistry, Indian Association for the Cultivation of Science. S.C. is thankful to the Council of Scientific and Industrial Research (CSIR), India, for a fellowship.

References

1. Costas M, Mehn MP, Jensen MP, Que L Jr (2004) Chem Rev 104:939–986
2. Hausinger RP (2004) Crit Rev Biochem Mol Biol 39:21–68
3. Purpero V, Moran GR (2007) J Biol Inorg Chem 12:587–601
4. Hegg EL, Que L Jr (1997) Eur J Biochem 250:625–629
5. Abu-Omar MM, Loaiza A, Hontzeas N (2005) Chem Rev 105:2227–2252
6. Que L Jr (2000) Nat Struct Biol 7:182–184
7. Straganz GD, Nidetzky B (2006) ChemBioChem 7:1536–1548
8. Koehntop KD, Emerson JP, Que L Jr (2005) J Biol Inorg Chem 10:87–93
9. Elkins JM, Ryle MJ, Clifton IJ, Hotopp JCD, Lloyd JS, Burzlaff NI, Baldwin JE, Hausinger RP, Roach PL (2002) Biochemistry 41:5185–5192
10. Price JC, Barr EW, Glass TE, Krebs C, Bollinger JM Jr (2003) J Am Chem Soc 125:13008–13009
11. Krebs C, Fujimori DG, Walsh CT, Bollinger JM Jr (2007) Acc Chem Res 40:484–492
12. Hoffart LM, Barr EW, Guyer RB, Bollinger JM Jr, Krebs C (2006) Proc Natl Acad Sci USA 103:14738–14743
13. Galonic DP, Barr EW, Walsh CT, Bollinger JM Jr, Krebs C (2007) Nat Chem Biol 3:113–116
14. Price JC, Barr EW, Tirupati B, Bollinger JM Jr, Krebs C (2003) Biochemistry 42:7497–7508
15. Proshlyakov DA, Henshaw TF, Monterosso GR, Ryle MJ, Hausinger RP (2004) J Am Chem Soc 126:1022–1023
16. Sinnecker S, Svensen N, Barr EW, Ye S, Bollinger JM Jr, Neese F, Krebs C (2007) J Am Chem Soc 129:6168–6179
17. Price JC, Barr EW, Hoffart LM, Krebs C, Bollinger JM Jr (2005) Biochemistry 44:8138–8147
18. Hoffart LM, Barr EW, Guyer RB, Bollinger JM Jr, Krebs C (2006) Proc Natl Acad Sci USA 103:14738–14743
19. Matthews ML, Krest CM, Barr EW, Vaillancourt FH, Walsh CT, Green MT, Krebs C, Bollinger JM Jr (2009) Biochemistry 48:4331–4333
20. Galonić Fujimori D, Barr EW, Matthews ML, Koch GM, Yonce JR, Walsh CT, Bollinger JM Jr, Krebs C, Riggs-Gelasco PJ (2007) J Am Chem Soc 129:13408–13409
21. Riggs-Gelasco PJ, Price JC, Guyer RB, Brehm JH, Barr EW, Bollinger JM Jr, Krebs C (2004) J Am Chem Soc 126:8108–8109
22. Bassan A, Borowski T, Siegbahn PEM (2004) Dalton Trans 3153-3162
23. Borowski T, Bassan A, Siegbahn PEM (2004) Chem Eur J 10:1031–1041
24. de Visser SP (2007) Chem Commun 171–173
25. Rohde J-U, In JH, Lim MH, Brennessel WW, Bukowski MR, Stubna A, Münck E, Nam W, Que L Jr (2003) Science 299:1037–1039
26. Lim MH, Rohde J-U, Stubna A, Bukowski MR, Costas M, Ho RYN, Münck E, Nam W, Que L Jr (2003) Proc Natl Acad Sci USA 100:3665–3670
27. England J, Martinho M, Farquhar ER, Frisch JR, Bominaar EL, Münck E, Que L Jr (2009) Angew Chem Int Ed 46:3622–3626
28. England J, Guo Y, Farquhar ER, Young VG Jr, Münck E, Que L Jr (2010) J Am Chem Soc 132:8635–8644
29. Que L Jr (2007) Acc Chem Res 40:493–500
30. Klinker EJ, Kaizer J, Brennessel WW, Woodrum NL, Cramer CJ, Que L Jr (2005) Angew Chem Int Ed 44:3690–3694
31. Kaizer J, Klinker EJ, Oh NY, Rohde J-U, Song WJ, Stubna A, Kim J, Nam W, Münck E, Que L Jr (2004) J Am Chem Soc 126:472–473
32. England J, Guo Y, Van Heuvelen KM, Cranswick MA, Rohde GT, Bominaar EL, Münck E, Que L Jr (2011) J Am Chem Soc 133:11880–11883
33. Chiou Y-M, Que L Jr (1995) J Am Chem Soc 117:3999–4013
34. Ha EH, Ho RYN, Kisiel JF, Valentine JS (1995) Inorg Chem 34:2265–2266
35. Hikichi S, Ogihara T, Fujisawa K, Kitajima N, Akita M, Morooka Y (1997) Inorg Chem 36:4539–4547
36. Chiou Y-M, Que L Jr (1994) Angew Chem Int Ed 33:1886–1888
37. Hegg EL, Ho RYN, Que L Jr (1999) J Am Chem Soc 121:1972–1973
38. Mehn MP, Fujisawa K, Hegg EL, Que L Jr (2003) J Am Chem Soc 125:7828–7842
39. Mukherjee A, Martinho M, Bominaar EL, Münck E, Que L Jr (2009) Angew Chem Int Ed 48:1780–1783
40. Mukherjee A, Cranswick MA, Chakrabarti M, Paine TK, Fujisawa K, Münck E, Que L Jr (2010) Inorg Chem 49:3618–3628
41. Paine TK, Zheng H, Que L Jr (2005) Inorg Chem 44:474–476
42. Paine TK, England J, Que L Jr (2007) Chem Eur J 13:6073–6081

43. Parkin G (2004) Chem Rev 104:699–768
44. Bruijnincx PCA, Lutz M, Spek AL, Hagen WR, Weckhuysen BM, van Koten G, Gebbink RJMK (2007) J Am Chem Soc 129:2275–2286
45. Bruijnincx PCA, van Koten G, Gebbink RJMK (2008) Chem Soc Rev 37:2716–2744
46. Paria S, Halder P, Paine TK (2010) Inorg Chem 49:4518–4523
47. Beck A, Weibert B, Burzlaff N (2001) Eur J Inorg Chem 521–527
48. Beck A, Barth A, Hübner E, Burzlaff N (2003) Inorg Chem 42:7182–7188
49. Burzlaff N (2008) Adv Inorg Chem 60:101–165
50. Cappillino PJ, Miecznikowski JR, Tyler LA, Tarves PC, McNally JS, Lo W, Kasibhatla BST, Krzyaniak MD, McCracken J, Wang F, Armstrong WH, Caradonna JP (2012) Dalton Trans 41:5662–5677
51. Friese SJ, Kucera BE, Que L Jr, Tolman WB (2006) Inorg Chem 45:8003–8005
52. Friese SJ, Kucera BE, Young VG Jr, Que L Jr, Tolman WB (2008) Inorg Chem 47:1324–1331
53. Dubois G, Murphy A, Stack TDP (2003) Org Lett 5:2469–2472
54. Ménage S, Vicent JM, Lambeaux C, Chottard G, Grand A, Fontecave M (1993) Inorg Chem 32:4766–4773
55. Ménage S, Vincent JM, Lambeaux C, Fontecave M (1994) J Chem Soc Dalton Trans 2081–2084
56. Duboc-Toia C, Menage S, Lambeaux C, Fontecave M (1997) Tetrahedron Lett 38:3727–3730
57. Bruker AXS (2006) APEX2, version 2.1-0. Bruker AXS, Madison
58. Farrugia LJ (1999) J Appl Crystallogr 32:837–838
59. Fox DB, Hall JR, Plowman RA (1962) Aust J Chem 15:235–241
60. König E, Ritter G, Madeja K (1981) J Inorg Nucl Chem 43:2273–2280
61. Chan BCK, Baird MC (2004) Inorg Chim Acta 357:2776–2782
62. Kahn O (1993) Molecular magnetism. VCH, New York
63. Ho RYN, Mehn MP, Hegg EL, Liu A, Ryle MJ, Hausinger RP, Que L Jr (2001) J Am Chem Soc 123:5022–5029
64. Shan X, Que L Jr (2005) Proc Natl Acad Sci USA 102:5340–5345
65. Maiti D, Lee D-H, Gaoutchenova K, Würtele C, Holthausen MC, Sarjeant AAN, Sundermeyer J, Schindler S, Karlin KD (2008) Angew Chem Int Ed 47:82–85